UDK 669.15:57.012.3:539.53
Original scientific article/Izvirni znanstveni članek

ISSN 1580-2949
Mater. Tehnol.

MICROSTRUCTURAL EVOLUTION AND HARDNESS OF FERRITIC SUPERALLOYS CONTAINING NiAl-B2 AND $L2_1$–Ni_2TiAl PRECIPITATES

MIKROSTRUKTURNI RAZVOJ IN TRDOTA FERITNIH SUPERZLITIN, KI VSEBUJEJO IZLOČKE NiAl-B2 in $L2_1$–Ni_2TiAl

Adi Ganda Putra[1], Selly Septianissa[2*], Pawawoi[3], Manty Aldilani Ikaningsih[3], Martoni[2], Martijanti[1], Mohammad Zaki Mubarok[4], Hafizh Ridwanulloh[3], Jodi Irawan[1], Ba'adilla Akhista Gamara[3]

[1]Machine Engineering, Faculty of Manufacturing Technology, Universitas Jenderal Achmad Yani, Bandung 40281, Indonesia
[2]Department of Mechanical Engineering, Faculty of Engineering, Widyatama University, Bandung 40125, Indonesia
[3]Metallurgical Engineering, Faculty of Manufacturing Technology, Universitas Jenderal Achmad Yani, Bandung 40281, Indonesia
[4]Department of Metallurgical Engineering, Faculty of Mining and Petroleum Engineering, Institut Teknologi Bandung, Jl. Ganesha 10, Bandung 40132, Indonesia

Prejem rokopisa – received: 2025-10-03; sprejem za objavo – accepted for publication: 2026-02-03

doi:10.17222/mit.2025.1575

This study investigates the effect of homogenization and aging treatments on the microstructure and hardness of ferritic superalloys containing NiAl-B2 and $L2_1$–Ni_2TiAl precipitates. Two alloy compositions were prepared using an electric arc furnace, with Ti additions of 2 *w*/% (Alloy I) and 4 *w*/% (Alloy II). The ingots were homogenized at 1150 °C for 10 h followed by furnace cooling, and subsequently aged at 800 °C for 8 h. Characterization was conducted using scanning electron microscopy (SEM) with energy-dispersive spectroscopy (EDS), X-ray diffraction (XRD), and Vickers hardness testing. The as-cast alloys exhibited the highest hardness, averaging 650.8 HV for Alloy I and 625.6 HV for Alloy II, due to the presence of metastable precipitates formed during rapid solidification. Homogenization reduced the hardness to 487.2 HV (Alloy I) and 522.6 HV (Alloy II) as a result of precipitate dissolution and redistribution of the alloying elements, while aging increased the hardness to approximately 525 HV in both alloys through secondary precipitation of the NiAl-B2 and $L2_1$–Ni_2TiAl with finer and more homogeneous distributions. SEM-EDS confirmed that Alloy I exhibited a more uniform dispersion of precipitates, whereas Alloy II contained a greater quantity of Ni_2TiAl, but with local agglomerations. In conclusion, homogenization and aging treatments strongly influenced the precipitation behavior and hardness of ferritic superalloys, with Alloy I showing superior homogeneity and Alloy II favoring greater Ni_2TiAl formation, highlighting the effect of Ti content on phase stability and mechanical performance.

Keywords: aging; ferritic superalloy; hardness; homogenization; $L2_1$–Ni_2TiAl; NiAl-B2; SEM; XRD

Namen študije, predstavljene v članku, je bil raziskati vpliv homogenizacije in staranja na mikrostrukturo in trdoto feritnih superzlitin, ki vsebujejo izločke NiAl-B2 in $L2_1$–Ni_2TiAl. Avtorji so pripravili dve zlitini v elektrobločni peči z dodatkom Ti v višini 2 *w*/% (zlitina I) in 4 *w*/% (zlitina II). Ingote obeh zlitin so 10 ur homogenizirali pri 1150 °C, jih ohladili v peči in nato starali 8 ur pri 800 °C. Za karakterizacijo izdelanih zlitin so uporabili vrstično elektronsko mikroskopijo (SEM) s prigrajenim energijskim disperzijskim spektroskopom (EDS), rentgensko difrakcijo (XRD) in Vickersov merilnik trdote. Ulite zlitine so imele najvišjo trdoto, zlitina I v povprečju 650,8 HV in zlitina II povprečno 625,6 HV, zaradi prisotnosti metastabilnih izločkov, ki so nastali med hitrim strjevanjem. Homogenizacija je zmanjšala trdoto na 487,2 HV (zlitina I) in 522,6 HV (zlitina II) zaradi raztapljanja izločkov in prerazporeditve legirnih elementov, medtem ko je staranje povečalo trdoto na približno 525 HV v obeh zlitinah zaradi sekundarnega izločanja NiAl s strukturo B2 in Ni_2TiAl s strukturo $L2_1$ z bolj fino in homogeno porazdelitvijo. SEM-EDS analiza je potrdila, da ima zlitina I bolj enakomerno porazdelitev izločkov, medtem ko je zlitina II vsebovala večjo količino Ni_2TiAl izločkov, vendar z lokalnimi aglomeracijami. Avtorji ugotavljajo, da sta homogenizacija in staranje močno vplivala na način izločanja in trdoto feritnih superzlitin, pri čemer je zlitina I pokazala boljšo homogenost, zlitina II pa je dajala prednost večji tvorbi Ni_2TiAl, kar poudarja vpliv vsebnosti Ti na fazno stabilnost in mehanske lastnosti.

Ključne besede: staranje, feritna superzlitina, trdota, homogenizacija, izločki $L2_1$–Ni_2TiAl, NiAl-B2, SEM, XRD

1 INTRODUCTION

Superalloys have been developed as high-performance materials due to their ability to maintain strength, stability, and corrosion resistance at elevated temperatures.[1,2] These alloys are extensively applied in turbines, energy-conversion systems, and other high-temperature environments where conventional steels fail.[3,4] The demand for more efficient power generation and renewable energy systems has further increased the need for advanced superalloys with superior mechanical and chemical stability.[5–7]

Among the various types, ferritic superalloys have attracted considerable attention because of their lower cost, higher thermal conductivity, and lower coefficient of thermal expansion compared to nickel-based superalloys.[8–10] These characteristics make ferritic alloys particularly suitable for structural applications exposed to cy-

*Corresponding author's e-mail:
selly.septianissa@widyatama.ac.id (Selly Septianissa)

clic thermal loads.[2] However, one of the limitations of ferritic alloys is their relatively lower creep and corrosion resistance at elevated temperatures. To overcome this, alloying strategies and precipitation strengthening have been introduced.

The addition of elements such as Ni, Al, and Ti plays a crucial role in forming intermetallic precipitates that enhance high-temperature performance. In particular, NiAl-B2 precipitates are known to provide effective strengthening through their coherent dispersion in the ferritic matrix.[11–13] Furthermore, the formation of $L2_1$–Ni_2TiAl precipitates contributes additional stability and resistance against dislocation motion, thereby improving both the mechanical strength and potential corrosion resistance. The balance between these precipitates is strongly influenced by the alloy composition and the applied heat treatments.[13–15]

Previous studies have shown that the ratio of Ni to Ti and the homogenization conditions determine the stability and morphology of these precipitates.[16,17] While NiAl-B2 tends to form during rapid cooling in the as-cast condition, $L2_1$–Ni_2TiAl usually emerges more prominently after controlled aging treatments.[18] The challenge lies in optimizing the precipitation sequence to achieve both uniform distribution and desired volume fraction, since excessive or uneven precipitation can lead to microsegregation and localized weaknesses.[19–22]

Heat treatment is a critical step in tailoring the microstructure of ferritic superalloys.[23] Homogenization eliminates chemical segregation and promotes the diffusion of alloying elements, but it may reduce hardness temporarily due to precipitate dissolution. Aging, on the other hand, refines and redistributes precipitates, restoring hardness through precipitation-hardening mechanisms.[24] Therefore, a systematic study on the homogenization–aging sequence is necessary to understand the microstructural evolution and its effect on mechanical properties.[25–27]

Recent reports have mainly focused on nickel-based or austenitic superalloys, while fewer works have addressed ferritic systems reinforced with Ni–Al–Ti precipitates.[11] Moreover, the majority of studies emphasized creep or oxidation resistance, with less attention given to the correlation between microstructure, hardness, and controlled precipitation of NiAl-B2 and $L2_1$–Ni_2TiAl in ferritic alloys. This creates a knowledge gap, particularly regarding how different Ti additions affect precipitation behavior during homogenization and aging.[12]

In this context, the present study investigated ferritic superalloys with two Ti variations (2 *w*/% and 4 *w*/%) prepared via electric arc melting. The alloys were subjected to homogenization at 1150 °C for 10 h and aging at 800 °C for 8 h to examine the evolution of precipitates and their effect on hardness. Microstructural analysis was performed using scanning electron microscopy (SEM) with energy-dispersive spectroscopy (EDS), and phase identification was carried out by X-ray diffraction (XRD). Vickers hardness testing was conducted to evaluate the mechanical response.

The objective of this work was to clarify the influence of heat treatment on the precipitation of NiAl-B2 and $L2_1$–Ni_2TiAl in ferritic superalloys and to establish the relationship between alloy composition, microstructure, and hardness. The findings provide essential insights into precipitation-strengthening mechanisms and highlight the role of Ti content in controlling the phase stability. This study contributes to the broader development of ferritic superalloys for high-temperature applications by providing fundamental knowledge of heat-treatment–microstructure–property relationships.

2 EXPERIMENTAL PART

The ferritic superalloys were synthesized by electric arc melting under an argon atmosphere to minimize any oxidation. Two compositions were designed with variations in titanium content, denoted as Alloy I (2 *w*/% Ti) and Alloy II (4 *w*/% Ti). The nominal chemical compositions of the alloys are presented in **Table 1**. High-purity raw materials of Fe, Ni, Cr, Al, Ti, Mo, and Zr (≤99.5 %) were used as starting elements. Each alloy was produced in button ingot form with a mass of approximately 15 g per button.

Table 1: Nominal chemical compositions of the ferritic superalloys (*w*/%)

Alloy	Fe	Cr	Ni	Al	Mo	Ti	Zr
I	68	10	10	6.5	3	2	0.25
II	66	10	10	6.5	3	4	0.25

The melting was conducted in a water-cooled copper crucible under continuous argon flow. Each ingot was flipped and remelted at least three times to ensure the compositional homogeneity. The resulting as-cast samples were subsequently cut into smaller specimens for heat treatment and characterization.

The heat treatment was performed in two stages. First, homogenization was conducted at 1150 °C for 10 h followed by furnace cooling to room temperature. This treatment was designed to minimize microsegregation and to redistribute alloying elements within the ferritic matrix. Second, aging was performed at 800 °C for 8 h followed by furnace cooling. This process was intended to promote secondary precipitation of NiAl-B2 and $L2_1$–Ni_2TiAl phases with refined morphology and improved distribution.

The homogenization temperature of 1150 °C was selected based on previous studies on Fe–Ni–Al–Ti ferritic superalloys, where this temperature was reported to effectively dissolve coarse intermetallic precipitates and minimize chemical segregation without excessive grain growth. The subsequent aging treatment at 800 °C for 8 h was chosen to promote the controlled secondary precipitation of NiAl-B2 and $L2_1$–Ni_2TiAl phases, which are

known to contribute to precipitation strengthening in similar alloy systems.

Microstructural characterization was carried out using scanning electron microscopy (SEM, JEOL JSM-IT200) equipped with energy-dispersive spectroscopy (EDS) to analyze elemental distribution and phase composition. X-ray diffraction (XRD, GGAS) with Cu Kα radiation (λ = 0.15406 nm) was employed for phase identification in the range 2θ = 20–90° with a step size of 0.02°.

The mechanical properties were evaluated by Vickers hardness testing (HV) using a load of 9.81 N (1 kgf) applied for 10 s. At least five measurements were taken for each sample, and the average values with standard deviations were calculated.

3 RESULTS

The hardness measurements of the ferritic superalloys under different conditions are summarized in **Table 2**. In the as-cast state, both alloys showed relatively high hardness values, with Alloy I reaching an average of 650.82 HV and Alloy II reaching 625.60 HV. These values are considerably higher than conventional ferritic steels, which generally exhibit hardness below 300 HV.

After homogenization at 1150 °C for 10 h, a decrease in hardness was observed. Alloy I decreased to 487.16 HV, while Alloy II decreased to 522.60 HV. This reduction indicated that the homogenization process influenced the dissolution of precipitates and resulted in softer matrices. Nevertheless, Alloy II maintained a higher hardness compared to Alloy I after homogenization, showing the influence of higher titanium content.

Following the aging process at 800 °C for 8 h, both alloys experienced an increase in hardness. Alloy I reached 525.6 HV and Alloy II reached 525.0 HV. Although these values did not exceed the as-cast condition, the hardness became more stable and uniform. The trend of hardness variation across different heat-treatment conditions is illustrated in **Figure 1**.

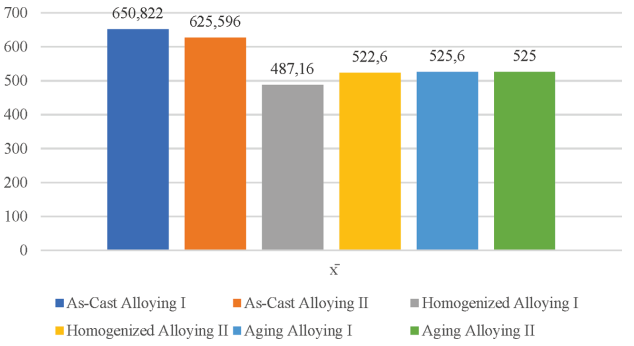

Figure 1: Hardness comparison of Alloy I and Alloy II in as-cast, homogenized, and aged conditions

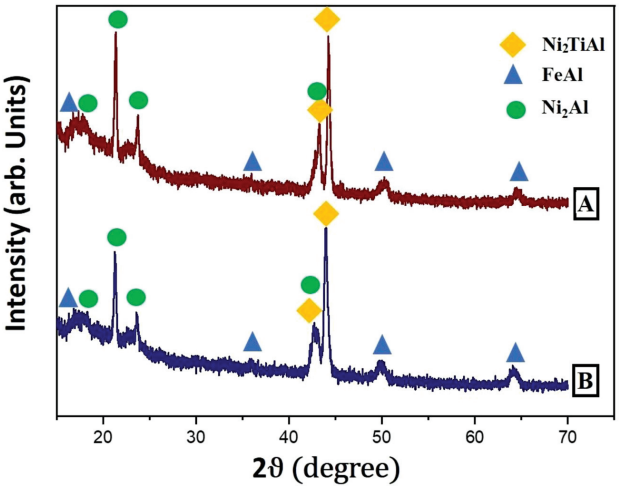

Figure 2: X-ray diffraction patterns of ferritic superalloys after homogenization: a) Alloy I (2 *w*/% Ti), b) Alloy II (4 *w*/% Ti)

Table 2: Hardness values of ferritic superalloys (HV) in as-cast, homogenized, and aged conditions

Condition	Alloy I (HV)	Alloy II (HV)
As-cast	650.82	625.60
Homogenized	487.16	522.60
Aged	525.60	525.00

The X-ray diffraction results of the alloys after homogenization are shown in **Figure 2**. Both alloys exhibited FeAl, Ni_2Al, and Ni_2TiAl phases. Alloy I showed a lower diffraction intensity for Ni_2TiAl, while Alloy II exhibited stronger diffraction peaks for this phase, suggesting a higher volume fraction of Ni_2TiAl due to the greater Ti addition. This difference highlighted the effect of composition on the precipitation behavior after homogenization.

After aging at 800 °C for 8 h, the diffraction patterns (**Figure 3**) revealed a noticeable increase in the intensity

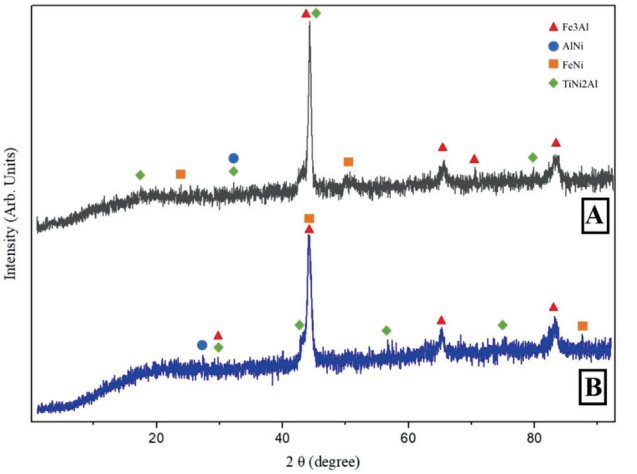

Figure 3: X-ray diffraction patterns of ferritic superalloys after aging at 800 °C for 8 h: a) Alloy I (2 *w*/% Ti), b) Alloy II (4 *w*/% Ti)

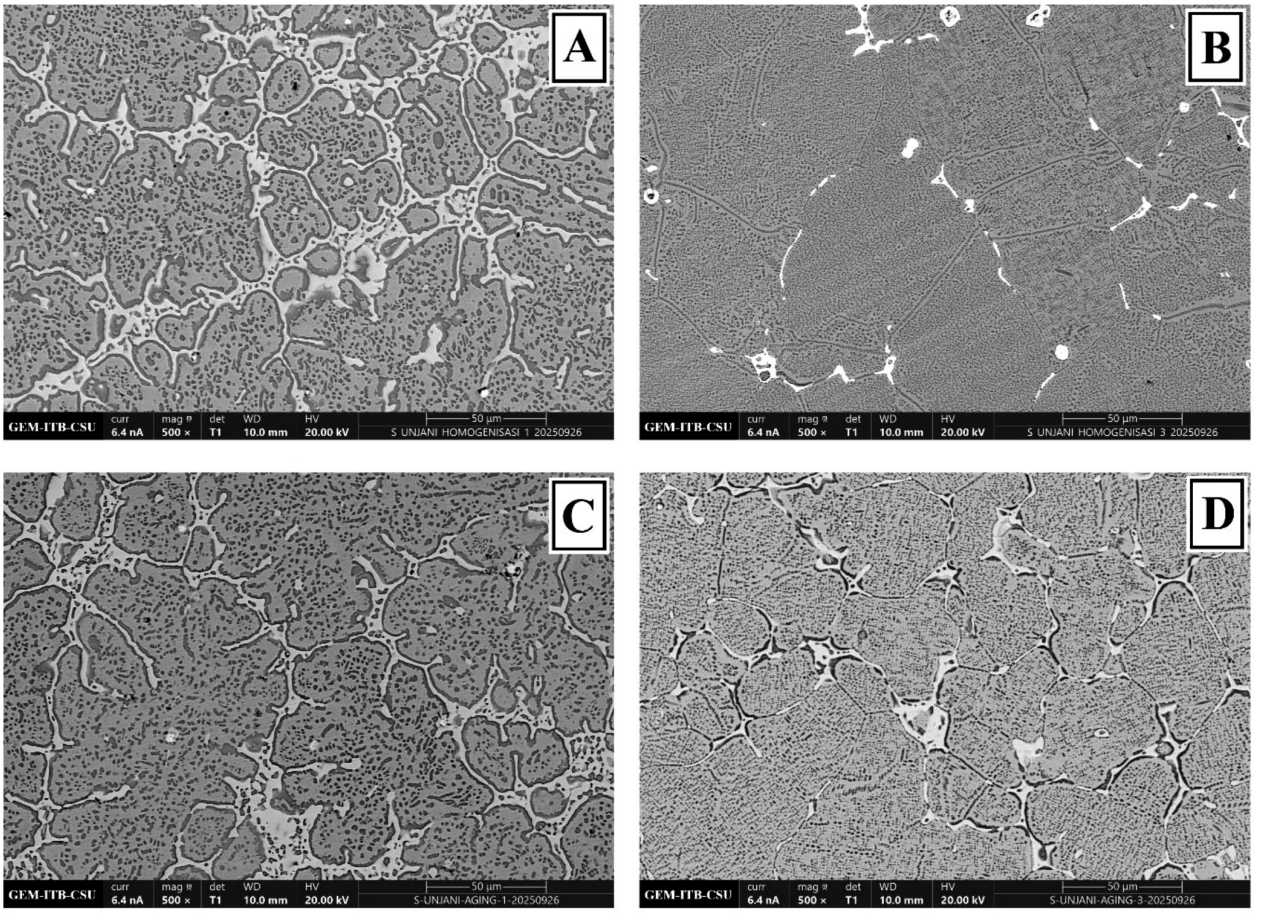

Figure 4: SEM micrographs of ferritic superalloys: a) homogenized Alloy I, b) homogenized Alloy II, c) aged Alloy I, d) aged Alloy II

of the Ni_2TiAl peaks for both alloys, indicating the formation and growth of secondary precipitates. Alloy II maintained stronger Ni_2TiAl reflections compared to Alloy I, confirming that a higher Ti content promotes further precipitation during aging. Meanwhile, Alloy I exhibited a slight enhancement in the NiAl-B2 phase, implying improved phase stability and homogeneity. The combined heat treatment process (homogenization followed by aging) thus facilitated both phase refinement and precipitation strengthening, which correlated with the increase in hardness observed experimentally.

Phase identification was performed by comparing the diffraction patterns with standard reference data (ICDD/JCPDS) and by correlating the XRD results with compositional information obtained from SEM-EDS analysis. Due to the potential overlap of diffraction peaks among FeAl, NiAl-B2, and $L2_1$–Ni_2TiAl phases, qualitative phase discrimination was supported by combined microstructural and elemental analysis, rather than relying solely on peak intensity.

The microstructural features of the alloys observed by SEM are presented in **Figure 4**. After homogeniza-

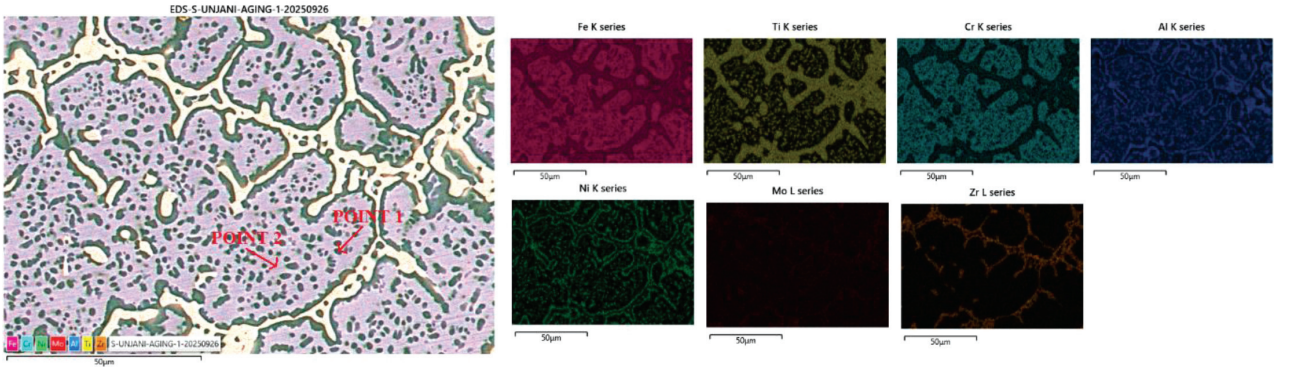

Figure 5: EDS elemental mapping of Alloy I after aging

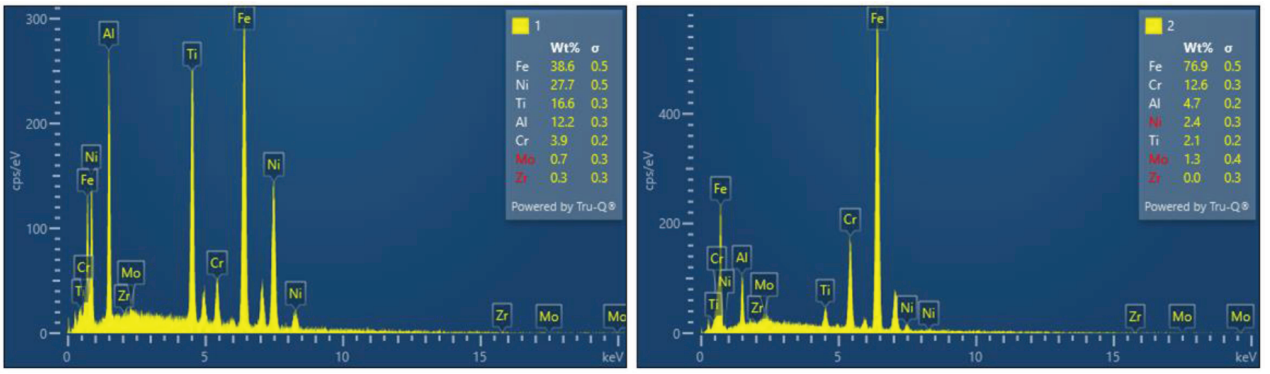

Figure 6: EDS elemental mapping of Alloy II after aging

tion, Alloy I showed relatively uniform ferritic grains with a fine dispersion of precipitates, while Alloy II exhibited a larger number of precipitates that were distributed less uniformly. After aging, the microstructures changed significantly. Both alloys exhibited refined grains and denser precipitate distributions. Alloy I displayed a more uniform and finer dispersion of precipitates, while Alloy II showed a larger quantity of precipitates, some of which tended to form clusters in localized regions.

The results of the EDS mapping are shown in **Figures 5** and **6**. In Alloy I, the main elements (Fe, Ni, Al, and Ti) were distributed relatively uniformly within the matrix. In Alloy II, however, there were localized regions enriched in Ni and Ti, corresponding to Ni_2TiAl precipitates. These observations suggested differences in precipitate formation between the two alloys depending on Ti content.

Quantitative EDS point analysis further clarified the microstructural differences, as presented in **Figures 7** and **8**. In Alloy I, Point 1 revealed the presence of Ni–Al–Ti enriched regions, whereas Point 2 showed Fe-rich ferritic regions. In Alloy II, Point 1 indicated enrichment of Zr together with Ni and Ti, while Point 2 showed predominantly Fe with limited amounts of Ni and Ti. These results demonstrated that Alloy II con-

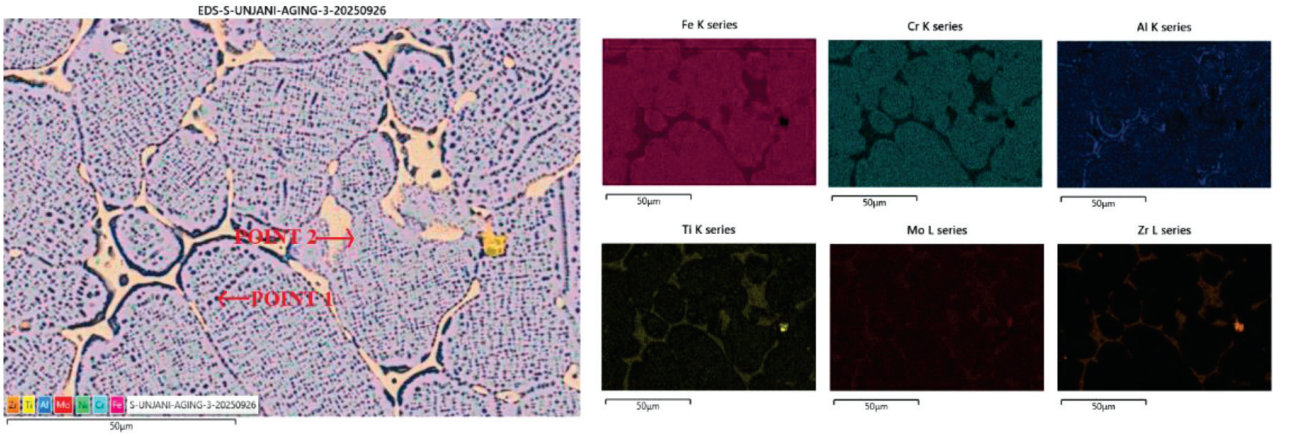

Figure 7: EDS point analysis of Alloy I (Point 1 and Point 2) after aging

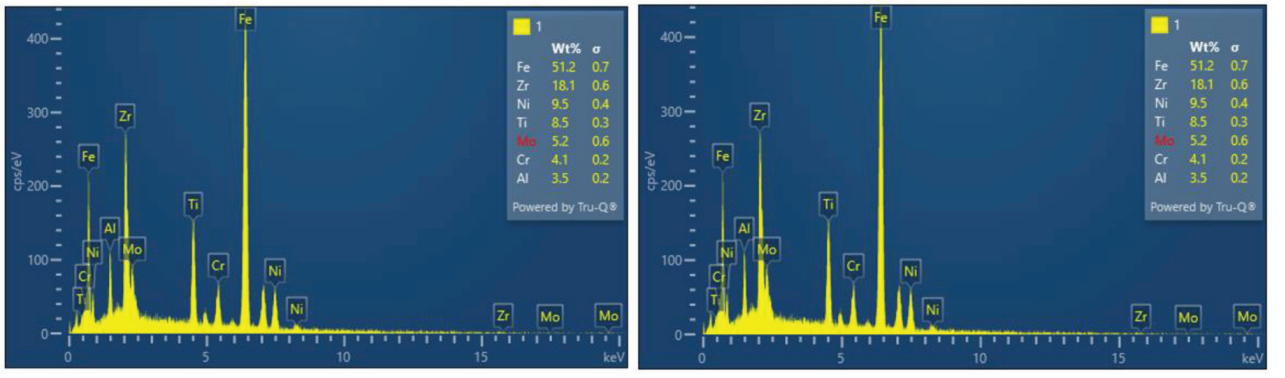

Figure 8: EDS point analysis of Alloy II (Point 1 and Point 2) after aging

tained not only higher Ti-related precipitates but also the localized segregation of secondary alloying elements such as Zr.

4 DISCUSSION

The evolution of hardness across different heat-treatment conditions can be directly correlated with the observed microstructural changes. In the as-cast condition, the presence of metastable precipitates formed during rapid solidification provides strong resistance to dislocation motion, resulting in high hardness values. Homogenization leads to precipitate dissolution and elemental redistribution, reducing hardness, while aging promotes the formation of finer and more stable NiAl-B2 and $L2_1$–Ni_2TiAl precipitates, which restore the hardness through precipitation-hardening mechanisms.

The results demonstrated that the hardness of ferritic superalloys was strongly influenced by both the composition and heat treatment. The highest hardness values were obtained in the as-cast condition, with Alloy I reaching 650.82 HV and Alloy II reaching 625.60 HV. These high values were attributed to the rapid-solidification process, which promoted the formation of metastable NiAl-B2 precipitates that effectively hindered dislocation motion. Such a phenomenon has been widely reported in ferritic and Ni–Al-based alloys, where rapid cooling leads to supersaturation and metastable strengthening phases.[28]

During homogenization at 1150 °C for 10 h, the hardness of both alloys decreased significantly. This reduction was caused by the dissolution of metastable precipitates and the redistribution of alloying elements into the ferritic matrix. Alloy I dropped to 487.16 HV, while Alloy II maintained a slightly higher value of 522.60 HV. The results indicated that higher Ti addition delayed the complete dissolution of Ni_2TiAl precipitates, which provided partial strengthening even after homogenization. Similar observations were reported by Wang et al. (2021), who found that Ti-rich ferritic alloys retain a fraction of Ni_2TiAl precipitates after high-temperature homogenization, resulting in moderate hardness retention.[16]

The aging treatment at 800 °C for 8 h restored the hardness values in both alloys, reaching approximately 525 HV. This recovery was associated with the secondary precipitation of NiAl-B2 and $L2_1$–Ni_2TiAl phases. The finer and more homogeneously distributed precipitates improved the hardness by providing effective barriers against dislocation glide through precipitation hardening. Alloy I exhibited slightly more uniform hardness values, while Alloy II showed higher scatter due to localized agglomeration of precipitates. These results confirmed that the controlled aging can refine the distribution of precipitates and compensate for the hardness loss caused by homogenization.

The XRD analysis supported these findings by revealing the coexistence of FeAl, Ni_2Al, and Ni_2TiAl phases after homogenization. The stronger Ni_2TiAl peaks observed in Alloy II confirmed that higher Ti addition favored the formation of this ordered intermetallic phase. Previous studies have also emphasized the role of Ti in stabilizing $L2_1$–Ni_2TiAl, which enhances high-temperature performance but requires careful control of distribution to avoid microsegregation. The balance between NiAl-B2 and Ni_2TiAl is therefore essential to achieve a desirable combination of strength and stability.[29]

After aging at 800 °C for 8 h, the XRD results revealed a clear increase in the intensity of Ni_2TiAl peaks for both alloys, indicating the continued precipitation of this phase during thermal exposure. This finding suggests that the diffusion of Ni, Ti, and Al atoms was enhanced during aging, promoting the formation of fine and ordered $L2_1$–Ni_2TiAl precipitates within the ferritic matrix. The appearance of stronger and sharper diffraction peaks also reflected an improvement in crystallinity and a reduction of lattice strain compared to the homogenized condition. The presence of FeNi and Fe_3Al peaks in minor proportions indicates a partial redistribution of Fe and Ni during the thermal treatment, a phenomenon consistent with typical diffusion-controlled phase evolution in Fe–Ni–Al–Ti systems.

Comparing both alloys, Alloy II showed a higher fraction and intensity of Ni_2TiAl after aging, confirming that Ti content has a direct influence on the precipitation kinetics. The excess Ti provided a higher driving force for the formation of $L2_1$–Ni_2TiAl, which contributes to enhanced high-temperature strength. However, this advantage may be offset by a tendency toward local compositional inhomogeneity, as excessive Ti can lead to microsegregation and the coarsening of intermetallics. In contrast, Alloy I exhibited a more balanced microstructure, where NiAl-B2 and Ni_2TiAl precipitates were more uniformly distributed, leading to better structural stability and moderate hardness improvement.

The synergistic role of homogenization and aging treatments can therefore be interpreted as a two-step precipitation process. Homogenization at 1150 °C for 10 h dissolved coarse intermetallics and promoted chemical uniformity, while subsequent aging at 800 °C for 8 h facilitated controlled precipitation and refinement of the $L2_1$–Ni_2TiAl phase. This sequence effectively combines matrix homogenization with precipitation hardening, which explains the improved mechanical performance measured experimentally. Such behavior is in agreement with previous reports on Fe–Ni–Al–Ti superalloys, where the dual presence of NiAl-B2 and Ni_2TiAl contributes to a superior strength and oxidation resistance at elevated temperatures.

Overall, the XRD and microstructural observations demonstrate that the Ti addition plays a key role in tailoring the balance between phase fraction and distribution. Alloy I, with lower Ti, favors homogeneity and structural integrity, while Alloy II, with higher Ti, enhances the amount of $L2_1$–Ni_2TiAl precipitates and po-

tentially improves high-temperature performance. The combination of these characteristics provides valuable insight for optimizing future compositions and heat-treatment parameters for ferritic superalloys designed for high-temperature applications.

SEM observations further clarified the differences between the two alloys. After homogenization, Alloy I displayed relatively uniform ferritic grains with fine precipitates, while Alloy II exhibited larger amounts of precipitates but with less homogeneous distribution. After aging, both alloys showed refined grains and denser precipitate distributions. Alloy I demonstrated more uniform dispersions, while Alloy II presented a higher quantity of precipitates that occasionally formed clusters. These microstructural differences explained the hardness trends, as uniform precipitate distributions tend to provide more consistent strengthening, while clustered precipitates may reduce overall efficiency despite their higher volume fraction.[30–33]

EDS mapping and point analysis confirmed these observations at the compositional level. Alloy I exhibited relatively homogeneous distributions of Fe, Ni, Al, and Ti, while Alloy II revealed localized enrichment of Ni and Ti corresponding to Ni_2TiAl precipitates. Point analysis of Alloy II also revealed significant enrichment of Zr in some regions, suggesting that Zr segregation may influence grain boundary stability and precipitate nucleation. These findings are in line with the work of Mayer et al. (2024), who reported that minor alloying additions such as Zr can play a critical role in refining grain size and enhancing the stability of intermetallic phases in ferritic alloys.[34]

Overall, the discussion of hardness, XRD, SEM, and EDS results highlighted the interplay between heat treatment, composition, and precipitation behavior. The as-cast condition promoted metastable strengthening, homogenization dissolved precipitates and reduced hardness, and aging restored hardness through refined secondary precipitation. Alloy I (2 *w*/% Ti) provided better homogeneity and more stable hardness response, while Alloy II (4 *w*/% Ti) promoted greater Ni_2TiAl formation but at the expense of uniformity. These results emphasize that careful optimization of Ti content and heat treatment conditions is required to achieve the best balance between strength and microstructural stability in ferritic superalloys.

Although Alloy II contains a higher Ti content and exhibits a larger volume fraction of $L2_1$–Ni_2TiAl precipitates, both alloys show comparable hardness values after aging. This behavior can be explained by the balance between precipitate volume fraction and distribution uniformity. Alloy I benefits from a finer and more homogeneous precipitate dispersion, while Alloy II shows partial precipitate clustering, resulting in a similar net strengthening effect.

5 CONCLUSIONS

Ferritic superalloys containing NiAl-B2 and $L2_1$–Ni_2TiAl precipitates were synthesized and heat treated with homogenization and aging. The as-cast alloys exhibited the highest hardness due to the presence of metastable precipitates formed during rapid solidification. Homogenization at 1150 °C for 10 h reduced the hardness as a result of precipitate dissolution and elemental redistribution, while subsequent aging at 800 °C for 8 h restored the hardness through the formation of finer and more stable secondary precipitates. Alloy I (2 *w*/% Ti) showed more homogeneous precipitate distributions, whereas Alloy II (4 *w*/% Ti) promoted higher amounts of Ni_2TiAl with local clustering. These findings demonstrated that Ti content and heat-treatment sequence played a decisive role in controlling precipitation behavior, microstructural stability, and mechanical response of ferritic superalloys.

Acknowledgment

The authors gratefully acknowledge the financial support provided by the Ministry of Education, Culture, Research, and Technology of the Republic of Indonesia through the BIMA research grant scheme. The authors also thank the research facilities at BRIN and Universitas Jenderal Achmad Yani for technical assistance and laboratory support during this work.

6 REFERENCES

[1] S. Septianissa, A. Z. Chandrasari, Behavior of Bare, Cr3C2-20NiCr, and NiCrAlY coated Fe-Ni Based Superalloy Under Hot Corrosion in a 75 wt.% Na2SO4 + 25wt.% NaCl film at 9000C, International Journal of Science and Society, vol. 6, no. 2, pp. 507–517, May 2024, doi:10.54783/ijsoc.v6i2.1170

[2] A. Ganda Putra, A. Manaf, A. Anawati, Enhancing the Hardness of Mg-9Al-1Zn Cast Alloy by Solution Treatment, IOP Conf Ser Mater Sci Eng, vol. 515, p. 012088, Apr. 2019, doi:10.1088/1757-899X/515/1/012088

[3] L. A. Morales, N. Luo, K. Li, C. H. Zenk, C. Körner, On stabilizing an $\alpha/\alpha'/\alpha''$ microstructure in ferritic superalloys, J Alloys Compd, vol. 911, p. 164996, Aug. 2022, doi:10.1016/j.jallcom.2022.164996

[4] J. E. Kanyo, S. Schafföner, R. S. Uwanyuze, K. S. Leary, An overview of ceramic molds for investment casting of nickel superalloys, J Eur Ceram Soc, vol. 40, no. 15, pp. 4955–4973, Dec. 2020, doi:10.1016/j.jeurceramsoc.2020.07.013

[5] J. E. Kanyo, S. Schafföner, R. S. Uwanyuze, K. S. Leary, An overview of ceramic molds for investment casting of nickel superalloys, J Eur Ceram Soc, vol. 40, no. 15, pp. 4955–4973, Dec. 2020, doi:10.1016/j.jeurceramsoc.2020.07.013

[6] P. M. Mignanelli et al., Gamma-gamma prime-gamma double prime dual-superlattice superalloys, Scr Mater, vol. 136, pp. 136–140, Jul. 2017, doi:10.1016/j.scriptamat.2017.04.029

[7] M. Sarikaya et al., A state-of-the-art review on tool wear and surface integrity characteristics in machining of superalloys, CIRP J Manuf Sci Technol, vol. 35, pp. 624–658, Nov. 2021, doi:10.1016/j.cirpj.2021.08.005

[8] S. Septianissa, B. Prawara, E. A. Basuki, E. Martides, E. Riyanto, Improving the hot corrosion resistance of γ/γ' in Fe-Ni superalloy coated with Cr3C2-20NiCr and NiCrAlY using HVOF thermal spray

coating, Int J Electrochem Sci, vol. 17, no. 12, p. 221231, Dec. 2022, doi:10.20964/2022.12.27

[9] J. Lauzuardy et al., Microstructure characteristics of Cr3C2-NiCr coatings deposited with the high-velocity oxy-fuel thermal-spray technique, Mater. Tehnol., 58 (**2024**) 2, doi:10.17222/mit.2023.869

[10] S. Septianissa, A. Z. Chandrasari, Corrosion Rate of ASTM A53 Steel in Seawater Influenced by Variation in Concentration of Mangifera Indica L. Peel Extract, Journal of Applied Engineering and Technological Science (JAETS), vol. 6, no. 1, pp. 550–560, Dec. 2024, doi:10.37385/jaets.v6i1.5182

[11] E. Pérez, C. Ferreira-Palma, H. J. Dorantes Rosales, V. López, M. A. Beltrán-Zúñiga, Aging Effect on Microstructural Evolution of B2(Nial) Coherent Precipitates in Ti-Modified Fe-Ni-Al Alloys, 2025. doi:10.2139/ssrn.5144878

[12] G. Zhao, X. Zang, W. Sun, Role of carbon in modifying solidification and microstructure of a Ni-based superalloy with high Al and Ti contents, Journal of Iron and Steel Research International, vol. 28, no. 1, pp. 98–110, Jan. 2021, doi:10.1007/s42243-020-00408-x

[13] W. C. Kim et al., Designing L2-strengthened Al-Cr-Fe-Ni-Ti complex concentrated alloys for high temperature applications, Acta Mater, vol. 211, p. 116890, Jun. 2021, doi:10.1016/j.actamat.2021.116890

[14] N. Luptáková, J. Svoboda, D. Bártková, A. Weiser, A. Dlouhý, The Irradiation Effects in Ferritic, Ferritic–Martensitic and Austenitic Oxide Dispersion Strengthened Alloys: A Review, Materials, vol. 17, no. 14, p. 3409, Jul. 2024, doi:10.3390/ma17143409

[15] F. Badkoobeh, H. Mostaan, M. Rafiei, H. R. Bakhsheshi-Rad, F. Berto, Microstructural Characteristics and Strengthening Mechanisms of Ferritic–Martensitic Dual-Phase Steels: A Review, Metals (Basel), vol. 12, no. 1, p. 101, Jan. 2022, doi:10.3390/met12010101

[16] Z. Wang et al., Coherent precipitation and stability of cuboidal B2 nanoparticles in a ferritic Fe–Cr–Ni–Al superalloy, Mater Res Lett, vol. 9, no. 11, pp. 458–466, Nov. 2021, doi:10.1080/21663831.2021.1973130

[17] Z. Wang, B. Jiang, H. Liu, B. Niu, H. Yu, Q. Wang, Microstructural Stability and Strengthening Mechanism of a Ferritic Fe–Cr–Ni–Al Superalloy Containing Cuboidal B2 Nanoparticles, 2023, pp. 469–485. doi:10.1007/978-3-031-27447-3_30

[18] X. Chen et al., Ductility deterioration induced by L21 phase in ferritic alloy through Ti addition, Journal of Materials Research and Technology, vol. 25, pp. 3273–3284, Jul. 2023, doi:10.1016/j.jmrt.2023.06.176

[19] K. Park et al., Developing high-strength ferritic alloys reinforced by combination of hierarchical and laves precipitates, J Alloys Compd, vol. 856, p. 158162, Mar. 2021, doi:10.1016/j.jallcom.2020.158162

[21] K. Park et al., Developing high-strength ferritic alloys reinforced by combination of hierarchical and laves precipitates, J Alloys Compd, vol. 856, p. 158162, Mar. 2021, doi:10.1016/j.jallcom.2020.158162

[21] U. B. Baek, J. Park, T. T. Nguyen, Effect of Elevated Temperature on Low Cycle Fatigue and Tensile Strength of 12Cr Ferritic Steel, Metals and Materials International, Dec. 2024, doi:10.1007/s12540-024-01858-8

[22] J. Kim et al., Designing L21-Co2TiAl precipitate-strengthened ferritic alloys with excellent high-temperature mechanical properties, Materials Science and Engineering: A, vol. 891, p. 145984, Jan. 2024, doi:10.1016/j.msea.2023.145984

[23] L. Verma, V. V. Dabhade, Investigation of nano-clusters evolved with Ti and Zr in ferritic ODS steel and their effect on microstructure and mechanical properties, Mater Today Commun, vol. 40, p. 109943, Aug. 2024, doi:10.1016/j.mtcomm.2024.109943

[24] S.-I. Baik, M. J. S. Rawlings, D. C. Dunand, Effect of aging on coarsening- and creep resistance of a Ti-modified Fe–Ni–Al–Cr–Mo ferritic steel with L21/B2 composite precipitates, Materials Science and Engineering: A, vol. 776, p. 138987, Mar. 2020, doi:10.1016/j.msea.2020.138987

[25] P. De Tiedra, Ó. Martín, M. San-Juan, Potentiodynamic study of the influence of gamma prime and eta phases on pitting corrosion of A286 superalloy, J Alloys Compd, vol. 673, pp. 231–236, Jul. 2016, doi:10.1016/j.jallcom.2016.02.261

[26] P. De Tiedra, Ó. Martín, M. San-Juan, Potentiodynamic study of the influence of gamma prime and eta phases on pitting corrosion of A286 superalloy, J Alloys Compd, vol. 673, pp. 231–236, Jul. 2016, doi:10.1016/j.jallcom.2016.02.261

[27] P. De Tiedra, Ó. Martín, M. San-Juan, Potentiodynamic study of the influence of gamma prime and eta phases on pitting corrosion of A286 superalloy, J Alloys Compd, vol. 673, pp. 231–236, Jul. 2016, doi:10.1016/j.jallcom.2016.02.261

[28] J. Xu et al., Continuous L21-Ordered Precipitation Induced Breakthrough of Strength and Ductility Trade-Off in Ni-Depleted Metastable High Entropy Alloy Under Quasi-State and Dynamic Compression, 2023. doi:10.2139/ssrn.4328091

[29] S. Li et al., Development and applications of aluminum alloys for aerospace industry, Journal of Materials Research and Technology, vol. 27, pp. 944–983, Nov. 2023, doi:10.1016/j.jmrt.2023.09.274

[30] T. Majeed, Y. Mehta, A. N. Siddiquee, Precipitation-dependent corrosion analysis of heat treatable aluminum alloys via friction stir welding, a review, Proc Inst Mech Eng C J Mech Eng Sci, vol. 235, no. 24, pp. 7600–7626, Dec. 2021, doi:10.1177/09544062211003609

[31] F. Godor et al., Microstructure Evolution of a New Precipitation-Strengthened Fe–Al–Ni–Ti Alloy down to Atomic Scale, Metals (Basel), vol. 12, no. 6, p. 906, May 2022, doi:10.3390/met12060906

[32] S. Wolff-Goodrich, A. Marshal, K. G. Pradeep, G. Dehm, J. M. Schneider, C. H. Liebscher, Combinatorial exploration of B2/L21 precipitation strengthened AlCrFeNiTi compositionally complex alloys, J Alloys Compd, vol. 853, p. 156111, Feb. 2021, doi:10.1016/j.jallcom.2020.156111

[33] M. S. Mehranpour, H. Shahmir, A. Derakhshandeh, M. Nili-Ahmadabadi, Significance of Ti addition on precipitation in CoCrFeNiMn high-entropy alloy, J Alloys Compd, vol. 888, p. 161530, Dec. 2021, doi:10.1016/j.jallcom.2021.161530

[34] J. A. Mayer, T. M. Pollock, K. V. Vamsi, R. Seshadri, Antiphase boundaries in B2 intermetallics: Proximate structures, formation energies, and chemical stability, Phys Rev Mater, vol. 8, no. 1, p. 013610, Jan. 2024, doi:10.1103/PhysRevMaterials.8.013610